Enhancing Security through Autonomous Learning Multi-Model Classification of 3D Palmprints: The ALMMo-0 Framework

Rezzag Aouid Fathi*, LATI Abdelhai, Chaa Mourad
Faculty of New information and communication technologies, Laboratory of Electrical Engineering
University Kasdi Merbah Ouargla (UKMO), BP 511, 30000, Ouargla, Algeria
E-mail: fathiaouid@gmail.com, lati.abdelhai@univ-ouargla.dz, chaa.mourad@univ-ouargla.dz

Keywords: biometric systems, 3D palmprint, classification accuracy, multi-scale retinex (MSR), local Phase quantization (LPQ), binarized statistical image features (BSIF), GIST descriptor, ALMMo-0 classifier

Received: July 10, 2024

As research progresses, biometric technologies have achieved notable effectiveness in personal identification. However, despite these advancements, there persists a demand for improved performance in security applications. ALMMo-0, the Autonomous Learning Multi-Model Classifier of zeroth order introduces a novel approach to address this challenge. It effectively addresses the challenges of Enhancing global efficiency in supervised 3D palmprint identification, autonomy, non-iterative procedures, and complete transparency. This study presents an innovative method Utilizing ALMMo-0 for enhancing 3D fingerprint-based authentication systems. The approach utilizes a feedforward methodology driven solely by data and non-iterative processes, leveraging three primary Techniques such as Local Phase Quantization (LPQ), GIST, and Binarized Statistical Image Information (BSIF) are employed to extract relevant details from three-dimensional palmprint images. Following feature extraction, ALMMo-0 autonomously generates AnYa Fuzzy Rule Base (FRB) sub-classifiers for individual categories, establishes a multimodal framework, and extracts data clouds. For authentication, the system utilizes a 'winner-takes-all' strategy for classifying incoming data, generating a confidence score that reflects the mutual distribution objectively. Tests performed on a 3D Palmprint dataset illustrate the efficacy of ALMMo-0, showcasing its performance using metrics Examples include metrics such as receiver operating characteristic (ROC) curves, rank-1 accuracy, equal error rate (EER), and cumulative match curve (CMC). The experimental evaluations demonstrate outstanding performance of the proposed method, achieving perfect rank-1 accuracy, minimal EER, and significant features such as interpretability and computational efficiency.

Povzetek: Prispevek predstavlja inovativni pristop z ALMMo-0, samoučečim klasifikatorjem, za izboljšanje 3D prepoznavanja dlani.

1 Introduction

The pervasiveness of social media and online networks presents a double-edged sword: fostering potential addiction while simultaneously serving as a cornerstone for businesses. Across these vast data landscapes, however, securing personal information remains paramount. Biometric systems address this concern by leveraging scientific methods, like iris scans and fingerprint recognition, to verify user identity through unique physical and behavioral traits. Among these techniques, 3D palmprint technology is particularly noteworthy, as evidenced by a growing body of research [1-2], attracting significant interest across diverse disciplines.

To address issues associated with 2D palmprint recognition systems, 3D palmprint-based personal recognition methods have recently been introduced [1–2]. For instance, Zhang et al. [3] proposed using Gaussian curvature images (GCI), mean curvature images (MCI), and surface type (ST) map features with matching metrics similar to Hamming distance. Additionally, Li et al. [4] presented a framework that extracts MCI from the original depth data along with baseline and orientation features. Despite these advancements, illicit access and advantages can still be gained by exploiting vulnerabilities in biometric systems [5]. Traditional 3D palmprint systems employing methods such as GCI and MCI also face challenges, including managing the growing number of registered templates and adapting to data distribution shifts, leading to high Equal Error Rates (EER) and reduced accuracy.

Conversely, incorporating score-level fusion with facial recognition offers a promising solution for advanced multi-modal 3D palmprint systems. This approach enables efficient processing of multiple templates and fosters adaptation through feedback adjustments, ultimately enhancing overall performance. Furthermore, a new method, Multiple Scale Recognition (MSR), which has not been used before, is proposed as a more robust alternative to classical methods like GCI and MCI, offering significant improvements in accuracy and reliability. Although biometric systems have advanced significantly, 3D palmprint technology has received

comparatively limited attention. Addressing these challenges, there is an urgent requirement to develop new 3D palmprint biometric systems to mitigate false acceptance rates and EER.

This paper proposes a novel biometric system utilizing the 0-order Autonomous Learning Multiple Model (ALMMo-0) classifier, specifically tailored for 3D palmprint recognition. The ALMMo-0 classifier, introduced by Angelov et al. (2017), offers a unique advantage in biometrics. Unlike traditional supervised machine learning methods that require constructing functions from training data, ALMMo-0 operates with complete autonomy. This is achieved through its multi-model framework, which continuously adapts its internal parameters based on incoming data without any prior assumptions.

Unlike conventional machine learning approaches that rely on training data with predefined categories, ALMMo-0, as introduced by Xing et al. in 2022, operates autonomously without requiring iterative parameter tuning or known category memberships. This is achieved through its feedforward architecture. By directly analyzing observational data, ALMMo-0 automatically identifies convergence points, eliminating the need for explicit training. It utilizes Voronoi Tessellation to construct fuzzy Rule-Based (FRB) AnYa subclassifies for each class directly from the non-parametric data. These subclassifiers assign confidence scores to incoming data samples. The final classification is determined by a "winner-takes-all" strategy, where the subclassifier with the highest confidence score assigns the class label to the new sample.

This research achieves two main advancements:

1. A New Biometric System for 3D Palmprints: The study proposes a novel biometric system specifically designed for 3D palmprint recognition. This system leverages the ALMMo-0 classifier, known for its efficient and autonomous operation without iterative training. The ALMMo-0 classifier itself is composed of a collection of fuzzy Rule-Based (FRB) AnYa subclassifiers.
2. Highly Effective ALMMo-0 Classifier: The research demonstrates the ALMMo-0 classifier's effectiveness through empirical testing on a dedicated dataset. The results show that the classifier achieves impressive accuracy with minimal errors. Additionally, it offers significant interpretability of its decision-making process, all while maintaining low computational complexity.

The remaining structure of the article follows a logical flow:

- **Section 2**: Background and Related Work - This section reviews existing research and relevant literature in the field.
- **Section 3**: Proposed System with ALMMo-0 - This section dives into the details of the proposed biometric system, focusing on the ALMMo-0 classifier's role.
- **Section 4**: Experiments and Analysis - This section presents the experimental results obtained by testing the proposed system and compares it to other approaches.
- **Section 5**: Conclusion and Future Work - The final section summarizes the key findings of the research and suggests potential areas for future exploration.

2 Related works

Biometric identity and recognition systems have seen significant advancements in both 2D and 3D palmprint technologies to meet growing security demands. Sun et al. [6] introduced the Orthogonal Line Ordinal Feature (OLOF) to improve stability in palmprint recognition. Zhang et al. [7] applied Hamming distance-based matching along with surface type maps (ST maps) and Gabor filters to enhance feature extraction. In 2010, Zhang et al. [8] developed a robust authentication system by merging 2D and 3D palmprint characteristics, leveraging surface curvature maps and normalized local correlation. Meanwhile, Yang et al. [9] proposed using Gabor wavelets and local binary patterns (LBP) to extract fine geometric details from 3D palmprints, while Li et al. [10] focused on joint line and orientation features to further improve recognition.

The shift towards multimodal systems began with Liu and Li [11], who tackled alignment challenges using a cross-correlation-based method alongside OLOF. Meraoumia et al. [12] introduced a multimodal biometric system integrating 2D and 3D palmprint data with PCA and Discrete Wavelet Transform (DWT) using Hidden Markov Models (HMM) for feature modeling. In 2014, Cui et al. [13] proposed a fusion-based system combining Principal Component Analysis (PCA) with a Two-Phase Test Sample Representation (TPTSR) for more accurate person recognition. Zhang et al. [14] presented collaborative representation techniques with block-wise feature extraction for enhanced 3D palmprint identification.

The trend towards advanced feature extraction continued with Chaa et al. [15], who employed Bank-Binarized Statistical Image Features (B-BSIF) and Gabor wavelets for score-level fusion. More recently, Chen et al. [16] proposed a hybrid multimodal system integrating finger vein and palmprint data for improved person identification. Li et al. [17] introduced a deep learning-based 3D palmprint system using CNNs, achieving robust performance even in real-time settings. Finally, Zhang et al. [18] utilized transformer-based models for palmprint recognition, setting new benchmarks for accuracy and efficiency in biometric recognition systems. **Table 1** provides a summary of key research contributions in the field, highlighting the different methodologies, features, and fusion techniques employed to advance 2D and 3D palmprint recognition systems.

Table 1: Summary of research efforts in 2D and 3D palmprint recognition systems

Methods	2D Features	3D Features	Matching Scheme	Fusion Scheme	Tasks	Years
Sun et al. [6]	Orthogonal Line Ordinal Feature (OLOF)	N/A	Cross-correlation and OLOF	Matching	Identification	2005
Zhang et al. [7]	Surface Type Maps (ST), PCA, Gabor Filters	ST Binary Features	Bitwise logical 'AND'	Matching	Verification	2008
Zhang et al. [8]	Surface Curvature Maps	Normalized Local Correlation	Matching	Matching	Verification	2010
Yang et al. [9]	Gabor Wavelets + Local Binary Pattern (LBP)	N/A	Score-level Fusion	Fusion	Recognition	2011
Li et al. [10]	Joint Line and Orientation Features	Extracted from MCI	Feature-level Fusion	Fusion	Recognition	2011
Liu and Li [11]	Mean Curvature Image (MCI)	Curvature Maps (MCI-based features)	Cross-correlation based	Fusion	Identification	2012
Meraoumia et al. [12]	PCA + Discrete Wavelet Transform (DWT)	2D+3D Palmprint Fusion	Hidden Markov Model (HMM)	Score-level Fusion	Recognition	2013
Cui [13]	PCA + Two-Phase Test Sample Representation (TPTSR)	N/A	Matching	Fusion	Recognition	2014
Zhang et al. [14]	Collaborative Representation Techniques	Block-wise Features	Matching	Fusion	Identification	2015
Chaa et al. [15]	Bank-Binarized Statistical Image Features (B-BSIF)	Gabor + Self-Quotient Images	Score-level Fusion	Fusion	Recognition	2017
Chen et al. [16]	Multimodal Palm + Finger Vein Data	2D + 3D Integration	Hybrid Matching	Score-level Fusion	Identification	2019
Li et al. [17]	CNN-based Features	3D Depth Maps	Deep Learning Matching	Feature-level Fusion	Recognition	2020
Zhang et al. [18]	Transformer-based Features	N/A	Deep Learning Matching	Feature-level Fusion	Recognition	2021

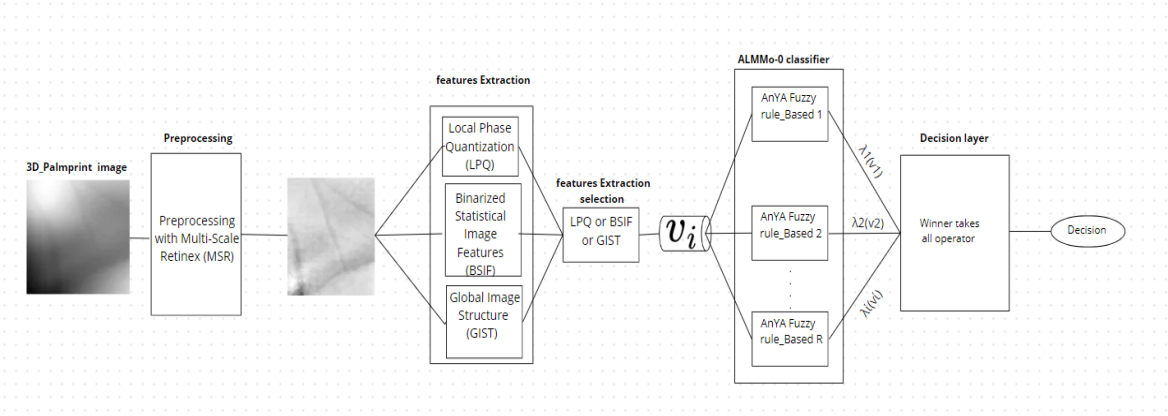

Figure 1: Diagram depicting the structure of the proposed method

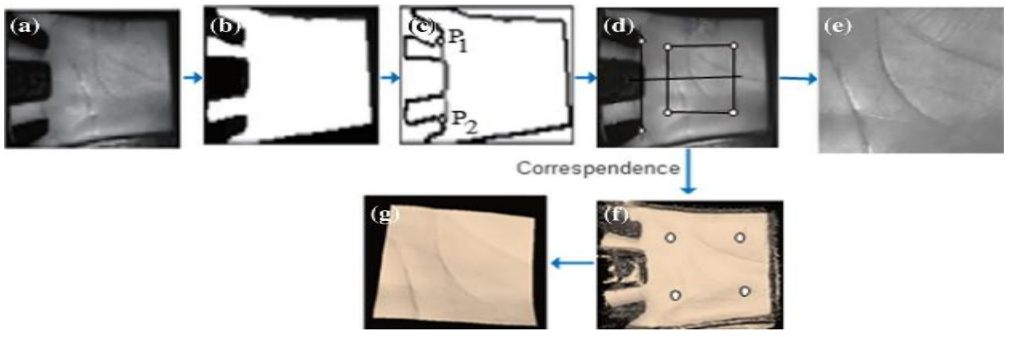

Figure 2: Extracting the region of interest (ROI) from a 3D palmprint image involves the following steps.

3 Proposed system

This study introduces an innovative biometric system for 3D palmprints, emphasizing the palmprint modality. At the heart of our methodology is the ALMMo-0 classifier, utilizing 0-order AnYa-type fuzzy rule-based (FRB) systems. Our approach integrates three specific descriptors—LPQ, BSIF, and GIST to capture essential features, which are then automatically classified by ALMMo-0. The system operates in a multi-stage process. First, it establishes a framework that incorporates different data modalities (multimodal framework) and identifies areas where these modalities come together (convergence points). Next, it leverages AnYa-like fuzzy rules to generate data representations independent of specific shapes (shape-free data clouds). These data clouds are then classified using sub-classifiers, each trained for a specific class and assigned a confidence score. Finally, the system employs a "winner-takes-all" approach to label additional samples. The effectiveness of this process is measured using metrics like False Acceptance Rate (FAR), Equal Error Rate (EER), True Positive Rate (TPR), Genuine Acceptance Rate (GAR), and Rank-1 accuracy. The proposed system employs a comprehensive architecture that integrates feature extraction techniques using LPQ, BSIF, or GIST filters. The classification task is handled by the ALMMo-0 classifier, which is supported by a Filter Bank descriptor for feature extraction. This architecture is illustrated in Figure 1, which outlines five primary phases. The first stage begins with capturing a 3D palmprint image, which undergoes preprocessing with multi-scale Retinex to improve image quality. The Filter Bank descriptor is employed to extract crucial features, utilizing either LPQ, BSIF, or GIST filters. These features form the basis for designing the classifier's model architecture. During feature extraction, the ALMMo-0 classifier acts as a gatekeeper, differentiating between legitimate users and imposters. The key to this biometric system lies in the Filter Bank, which meticulously selects relevant features from the data stream. ALMMo-0 operates in a sequential manner for autonomous data classification. It first builds multimodal representations and basic linguistic rules by analyzing the provided data. Then, it generates non-parametric data clusters, locates convergence zones, and leverages fuzzy rules extracted from these clusters to construct AnYa-type sub-classifiers for each category. Finally, ALMMo-0 assigns confidence levels to each class and employs a "winner-takes-all" strategy to label new data samples. To ensure accuracy, it evaluates its performance before delivering the final classification.

3.1 The region of interest

This section focuses on extracting the Region of Interest (ROI) from 3D palmprint data. Li et al. [19] employed a structured-light technology-based 3D acquisition system, enabling concurrent capture of 2D and 3D palm images (Figure 2). The ROI extraction process involves several steps. First, a Gaussian smoothing filter is applied to the original image, followed by thresholding using an automatically determined threshold T (Figure 2a, 2b). Otsu's method [20] facilitates this automatic threshold selection, converting the grayscale image to a binary representation. Next, a border tracking technique (Figure 2c) is employed to efficiently extract the boundaries of the binary image. By analyzing this boundary information, points P1 and P2 are identified to define the 2D ROI template. Finally, a rectangle is used to delineate and mark the ROI (Figure 2d). Figure 2e showcases the extracted 2D ROI, while Figure 2f presents the original 3D palmprint. The final 3D ROI is obtained by aligning the cloud points corresponding to the 2D ROI pixels, as detailed in [21].

3.2 Pre-processing

In the preprocessing phase, Multiscale Retinex (MSR) is applied. Retinex theory, originally formulated by Land and McCann [22], aims to replicate the human visual system's processing of visual information. Their work demonstrated that the visual system perceives relative lightness, focusing on variations in brightness within local image regions rather than absolute lightness levels. Multiscale Retinex (MSR) is particularly noted for its ability to achieve high-quality color rendition and a broad local dynamic range. The MSR output results from a weighted combination of outputs produced by multiple Single Scale Retinex (SSR) processes. Jobson et al. [23] further refined the formulation of multiscale Retinex based on these principles.

$$\mathbf{R_{MSR_i}} = \sum_{\mathbf{n=1}}^{\mathbf{N}} \boldsymbol{\omega_n} \mathbf{R_{n_i}} = \sum_{\mathbf{n=1}}^{\mathbf{N}} \boldsymbol{\omega_n} [\mathbf{log I_i}(\mathbf{x}, \mathbf{y}) - \mathbf{log}(\mathbf{F_n}(\mathbf{x}, \mathbf{y}) * \mathbf{I_i}(\mathbf{x}, \mathbf{y}))] \quad (1)$$

Where N represents the number of scales, ω_n indicates the weight assigned to each scale, and $I_i(x, y)$refers to the input image on the i-th color channel. R_{MSR_i} denotes the output image from Retinex processing on the i-th color channel. F represents the normalized surround function. Figure 3 shows the original images of various individuals before applying Multiscale Retinex (MSR) and the results obtained after the application of Multiscale Retinex (MSR).

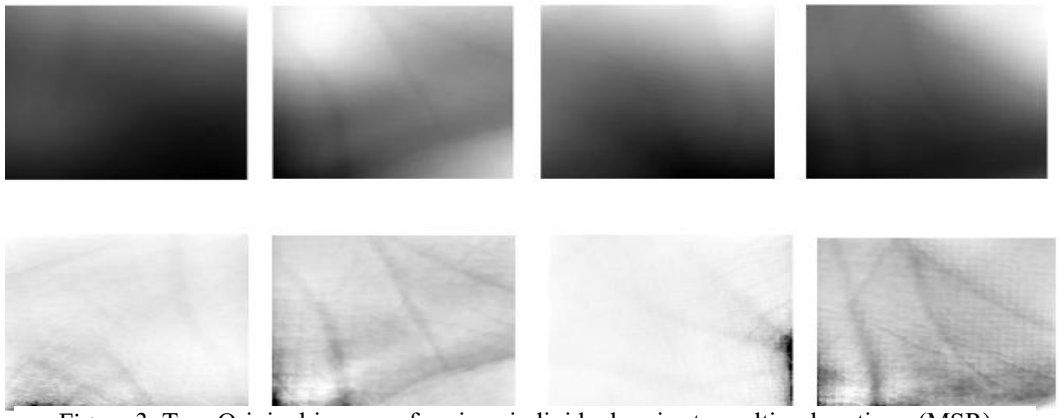

Figure 3: Top: Original images of various individuals prior to multiscale retinex (MSR) application. bottom: results obtained after applying multiscale retinex (MSR).

3.3 Feature extraction

The process of feature extraction using LPQ, BSIF, or GIST descriptors entails identifying and isolating salient features from a broad spectrum of image characteristics. In-depth descriptions of each descriptor are presented in the following subsections:

3.3.1 Local phase quantization (LPQ)

Ojansivu's LPQ method exploits the phase of the Fourier transform in localized regions to induce spatial blurring. This technique achieves blurring by applying a point spread function (PSF) to attenuate image intensity, analogous to multiplication in the frequency domain.

$$\mathbf{G(u) = F(u) \cdot H(u)} \tag{2}$$

Considering only the phase spectra, the Fourier transforms G(u), H(u), and F(u) of the blurred image, point spread function (PSF), and original image, respectively, exhibit a summation relationship.

$$\mathbf{\angle G(u) = \angle F(u) + \angle H(u)} \tag{3}$$

where ∠G(u), ∠H(u) and ∠F(u) are phase angle of G(u), H(u) and F(u), respectively. If PSF is centrally symmetric, namely h(x) = h(−x), the transform H(u) becomes real valued and the phase angle ∠H(u)can be represented by a two-valued function:

$$\mathbf{\angle H(u)} = \begin{cases} \mathbf{O \text{ if } \angle H(u) > o} \\ \mathbf{1 \text{ if } \angle H(u) < o} \end{cases} \tag{4}$$

In all angles where ∠H(u)≥0, if ∠G(u)=∠F(u) and considering the shape of H(u) resembling a regular Point Spread Function (PSF) like Gaussian or sinc-function, it ensures that low-frequency values of ∠H(u) remain non-negative at a minimum. These frequencies maintain ∠G(u)= ∠F(u), ensuring that ∠F(u) remains invariant to blurring. In the LPQ scheme, M-by-M local neighborhoods $\boldsymbol{Nx}$ filters are applied at each pixel position of the image f(x) to analyze the phase. The local spectrum is obtained using a short-term Fourier transform.

$$\mathbf{F(u,x)} = \sum_{\mathbf{y \in N_x}} \mathbf{f(y-x)} e^{\mathbf{j2\pi u T_y}} \tag{5}$$

To efficiently compute the transformation at each image location (x ∈ {X1, X2, ..., XN}), we leverage 1D convolutions. These convolutions are applied sequentially to both the rows and columns of the image. This approach allows us to calculate local Fourier coefficients at four specific frequency points: $u_1 = [a, 0]^T$, $u_2 = [0, a]^T$, $u_3 = [a, a]^T$, and $u_4 = [a, -a]^T$. Here, 'a' is a carefully chosen small scalar that ensures $H(u_i) \geq 0$ for all i (i = 1, 2, 3, 4). As a result, we obtain a vector for every pixel position.

$$\mathbf{F(x)} \left(\begin{bmatrix} \mathbf{Re\{F(u_1,x), Im(u_1,x)\}}, \ldots \\ \mathbf{[Re\{F(u_1,x), Im(u_1,x)\}]} \end{bmatrix} \right) \tag{6}$$

The phase of each Fourier coefficient is encoded by the signs of its real and imaginary parts. This can be extracted using simple scalar quantization.

$$\mathbf{q_j} = \begin{cases} \mathbf{1}, & \mathbf{if\ f_i > 0} \\ \mathbf{0}, & \mathbf{if\ f_i < 0} \end{cases} \tag{7}$$

3.3.2 Binarized statistical image features (BSIF)

BSIF (Binarized Statistical Image Features) is a technique introduced in [21] that assigns a binary code string to each pixel in an image. This binary code represents the local descriptor for that pixel. The filter response R_i for an image I_p and a corresponding linear filter of the same size Wi is calculated as follows:

$$R_i = \sum_{m,n} I_p(m,n)\, W_i(m,n) \tag{8}$$

The equation utilizes m and n to represent the patch size in Patch Per Inch (PPI). $\forall i \in \{1,\ldots, n\}$. Filters is denoted by $W_i(m,n)$. The filter responses are calculated and binarized, generating a binary string as described in [22].

$$b_i = \begin{cases} 1 & if\ R_i > o \\ 0 & otherwise \end{cases} \tag{9}$$

3.3.3 Gist descriptor

To tackle scene classification challenges, the GIST descriptor [24] proves effective. It achieves this by leveraging Gabor filters, which analyze scenes using localized frequency information. These filters offer a

compressed and efficient feature representation. In our work, we utilized GIST descriptors with 8 orientations across 5 scales and a 6x6 grid to extract features. This involved convolving each image with a set of Gabor filters spanning the specified orientations and scales, resulting in feature vectors. Mathematically, In the spatial domain, a Gabor filter is formed by multiplying a complex sinusoid with a Gaussian envelope. This operation essentially defines a 2D Gabor filter with the function $\boldsymbol{H_{\mu,v}}$ representing it.

$$\boldsymbol{H_{\mu,v}} = \frac{\boldsymbol{f_\mu^2}}{\boldsymbol{\pi n \lambda}} \boldsymbol{exp}\left[-\left(\frac{\boldsymbol{f_\mu^2}}{\boldsymbol{n^2}}\right)\boldsymbol{x_p^2} - \left(\frac{\boldsymbol{f_\mu^2}}{\boldsymbol{\lambda^2}}\right)\boldsymbol{y_p^2}\right] \boldsymbol{exp}(\boldsymbol{j2\pi x_p}) \quad (10)$$

With $x_p = xcos(\theta v) + ysin(\theta v)$ and $y_p = -x\,sin(\theta v) + y\,cos(\theta v)$.The parameters of Gabor filter are: $yp = -xsin(\theta v) + ycos(\theta v)$ $f_\mu = \frac{f_{max}}{\frac{\mu}{2^2}}$ and $\theta_v = {}^{v\pi}/_{8}$

Where: $f\mu$ = center frequency, f_{max} = maximal frequency and θ_v = orientation

To capture multi-scale orientation information, 2D Gabor filters were employed with fmax set to 0.25 and $\boldsymbol{n} = \boldsymbol{\lambda} = \sqrt{2}$, where $\boldsymbol{n}$ and $\boldsymbol{\lambda}$ represent the Gaussian envelope's size along the x and y axes, respectively. These Gabor filters generate feature maps that encode orientation information at various scales, effectively capturing the image's intricate spatial structure and characteristics.

3.4 Reduction of the dimensionality

High-dimensional data, characterized by numerous feature vectors, can pose hurdles for processing and classification tasks. To overcome these challenges, dimensionality reduction techniques come into play. These methods offer several advantages: managing large datasets more efficiently, enhancing prediction accuracy, reducing computational time, and unlocking a deeper understanding of the data itself. A popular and effective approach is Linear Discriminant Analysis (LDA). LDA seeks to find a transformation matrix, denoted by W, that optimizes the separation between classes while simultaneously minimizing variation within each class [25-26].

$$T(W) = W_{opt} = arg_W max \frac{|W^T S_B W|}{|W^T S_T W|} = [W_1 W_2 \ldots\ldots W_d] \quad (11)$$

The Fisher discriminant criterion, denoted as T(W), is maximized by constructing the matrix W through concatenating the top d eigenvectors. This matrix W is obtained by solving the following equation:

$$S_W^{-1} S_B W_j = W_j \lambda_j \quad (12)$$

In this study, Linear Discriminant Analysis (LDA) was chosen as the primary dimensionality reduction technique due to its focus on maximizing class separability, which is crucial for 3D palmprint recognition. Unlike Principal Component Analysis (PCA), which reduces dimensionality by preserving variance without considering class labels, LDA explicitly optimizes for separation between different classes. This makes LDA more suitable for supervised learning tasks where distinct classification boundaries are essential. While t-SNE is effective for visualizing high-dimensional data by projecting it into lower-dimensional space, it is primarily used for unsupervised learning and exploratory data analysis. t-SNE tends to emphasize local structure, making it less ideal for classification tasks where global class separability is needed, especially when working with larger datasets and multiple classes. LDA was selected because its primary objective is to maximize the between-class variance while minimizing the within-class variance, making it well-suited for this study where the focus is on ensuring robust class separability between different palmprint features. The experimental results demonstrated that LDA, in combination with the ALMMo-0 classifier, led to optimal performance in terms of accuracy and Equal Error Rate (EER), outperforming PCA and t-SNE in this context.

3.5 The ALMMo-0 classifier

The core of the proposed 3D palmprint biometric system lies in the ALMMo-0 classifier, a novel machine learning approach. This classifier autonomously builds a multi-model framework from experimental data. The design hinges on two key steps: **1)** Automatic identification of focal points and generation of individual data clouds through Voronoi Tessellation [27]. **2)** Construction of AnYa Fuzzy Rule-based (FRB) sub-classifiers for each class, utilizing these data clouds for classification of new data points. The initial stages of the ALMMo-0 classifier architecture are depicted in Figure 4. Table 2 shows the symbols used in the ALMMo-0 classifier. Figure 4 highlights four key components:

1. Data Preprocessing: This layer normalizes the incoming data, ensuring optimal performance and improved classifier functionality.
2. AnYa Fuzzy Rule-based Sub-classifiers: This layer leverages non-parametric data to construct a collection of sub-classifiers, each utilizing AnYa fuzzy rules.
3. Winner Selection: This layer employs a "winner-takes-all" strategy to classify new data points. The classification is based on confidence scores provided by each sub-classifier.
4. Class Assignment: This layer assigns a class label to new data samples based on their strongest likelihood of belonging to a specific class.

Table 2: Explanation of symbols used in the ALMMo-0 classifier

Notation.	Signification
x^{*i}	The point of convergence-
$Class^i$	The class assigned to the i-th dataset -
R	The number of fuzzy rules -
C	A variety of classes across the dataset-
R^d	Euclidean space for data -
i	Dataset observed at the i-th instance -
k	Incoming data -
k	The average of all data samples at the K-th instance -
λ_i	Confidence level -
x_k^i	The kth normalized data point in the i-th class -
μ_k	Overall average -
$D_k(x_i)$	Density of the i-th data sample at time k, under a single-mode - distribution
X_{kk}	Average scalar product -
$M_{F^i}^{*i}$	Number of members in data clouds -
$r_{F^i}^{*i}$	Influence radius in the area -
x_N^{*i}	The convergence point where the nearest data cloud converges -
F^i	Count of convergence instances -

Algorithm 1: The fundamental algorithm of the ALMMo-0 classifier

While there is a novel coming data simple

i. **Normalization**

$$x_k^i \leftarrow \frac{x_k^i}{\|x_k^i\|}$$

ii. **Initialization**

IF $(k = 1)$**THEN**

$$\mathbf{1}.\,\mu_1^i \leftarrow x_1^i\ \mathbf{2}.\,F^i \leftarrow \mathbf{1}\ \mathbf{3}.\,M_1^{*i} \leftarrow \mathbf{1}\ \mathbf{4}.\,x_1^{*i} \leftarrow x_1^i\ \mathbf{5}.\,r_1^{*i} \leftarrow r_0$$

iii. Classification

ELSE

1. $Updating\ \mu_{k-1}^i\ to\ \mu_k^i$: $\mu_k = \frac{k-1}{k}\mu_{k-1} + \frac{1}{k}x_k$: $\mu_1 \leftarrow x_1$

2.Calculate the unimodal density $D_k\ of\ the\ data\ sample\ x_k^i$:

$$D_k(x_i) = \frac{1}{1+\frac{\|x_i-\mu_k\|^2}{\sigma_k^2}} = \frac{1}{1+\frac{\|x_i-\mu_k\|^2}{X_k-\|\mu_k\|^2}}$$

3.Update $D_k(x_k^{*i})(j = 1, 2 \ldots\ldots F^1)$

$$D_k(x_i) = \frac{1}{1+\frac{\|x_i-\mu_k\|^2}{\sigma_k^2}} = \frac{1}{1+\frac{\|x_i-\mu_k\|^2}{X_k-\|\mu_k\|^2}}$$

$$\mathbf{4}.\,IF\left(D_k(x_k^i) > max_{j=1.2\ldots F}\left(D_k\left(x_j^{*f}\right)\right)\right) or \left(D_k(x_k^i) < max_{j=1.2\ldots F}\left(D_k\left(x_j^{*f}\right)\right)\right) THEN$$

– **Create a new data cloud around** x_k^i **and initialize the parameters** :

$$F^1 \leftarrow F^1 + 1\ ; x_{F^i}^{*i} \leftarrow x_k^i\ ;\ M_{F^i}^{*i} \leftarrow 1\ ;\ r_{F^i}^{*i} \leftarrow r_0$$

5. Else

– **Find the nearest data cloud to** x_k^i :

$$x_N^{*i} \leftarrow argmin_{j=1.2...F^i}(\|x_k^i - x_j^{*i}\|);$$

- **IF** $(\|x_k^i - x_N^{*i}\|) \leq r_N^{*i}$ ***THEN***
- **Update the meta parameters of the data cloud** :

$$x_N^{*i} \leftarrow \frac{M_N^{*i}}{M_N^{*i}+1} x_N^{*i} + \frac{1}{M_N^{*i}+1}; r_N^{*i} \leftarrow \sqrt{0.5((r_N^{*i})^2 + (1 - \|x_N^{*i}\|^2))} \ ;$$

- **ELSE add new data cloud** : $F^1 \leftarrow F^1 + 1$; $x_{F^i}^{*i} \leftarrow x_k^i$; $M_{F^i}^{*i} \leftarrow 1$; $r_{F^i}^{*i} \leftarrow r_0$
- **ENDIF**

6.ENDIF
ENDIF
END WHILE

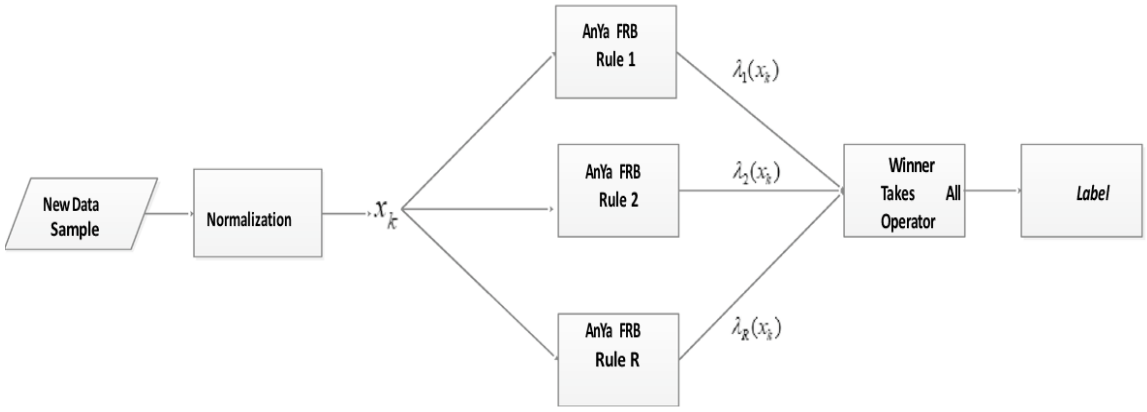

Figure 4: Graphical depiction illustrating the ALMMo-0 classifier within a block diagram

The ALMMo-0 classification process is data-driven and unfolds in a series of steps.

1. Data preprocessing: Prior to analysis, all input data undergoes normalization, where each sample is divided by its own norm. This ensures all data points are on a similar scale.

2. Initial model generation: The first data point becomes the foundation for the initial model, with its support (significance) set to 1.

3. Data cloud construction: Subsequent data points are assigned to the most relevant class using confidence scores generated by sub-classifiers. These classifications establish "data clouds" representing clusters of similar data points.

4. Dynamic model update: The algorithm continuously monitors the global data density. If a new data point falls outside the established density range (too high or low), a fresh data cloud is created around it. Otherwise, the existing data cloud closest to the new point is identified and updated by adjusting its support and radius to incorporate the new information.

5. Classification: Finally, the classifier leverages the constructed data clouds and associated confidence scores to determine the final class label for a new data point.

The ALMMo-0 procedure establishes a robust framework for 3D palmprint biometric systems by achieving accurate and efficient data categorization through a four-step process. These steps include:

1. **Normalization:** This initial phase standardizes the input data, ensuring consistency for further analysis.
2. **Meta-Parameter construction:** Here, the normalized data is leveraged to construct meta-parameters, which will be instrumental in the classification stage.
3. **Classification:** This stage utilizes the calculated global density and mean values to classify the data points.
4. **Validation:** Finally, validation data is routed to individual AnYa FRB sub-classifiers, which then generate the final labels for the data. This revised version emphasizes the overall functionality of ALMMo-0 and clarifies the role of each step within the system.

3.5.1 Computational complexity of the ALMMo-0 classifier

One of the key advantages of the ALMMo-0 framework is its ability to scale effectively with larger datasets and an increasing number of classes. The time complexity of the identification function, F(P×J×H), where P represents the number of data samples, J the number of data clouds, and H the number of features, ensures that the system scales efficiently as these factors grow. Furthermore, the verification function operates with a time complexity of F(P×J), making it highly adaptable to real-time classification tasks.

The space complexity, F(P×H), is similarly manageable, requiring only space to store the input data. As a result, the ALMMo-0 classifier can handle large-scale environments, such as national identification systems or corporate security databases, without significant computational overhead. Unlike traditional methods like PCA and SVM, which have complexities ranging from $F(T^2 \times R)$ to $F(T^3 \times R)$ (where T is the number of training samples and R is the number of features), ALMMo-0's lower complexity allows it to maintain high accuracy and low Equal Error Rate (EER) without the need for iterative tuning or retraining.

This combination of linear or sub-linear time and space complexity, along with the framework's ability to dynamically adapt to data distribution changes, ensures that the ALMMo-0 classifier remains efficient and scalable even under more demanding conditions.

3.5.2 Confidence thresholding

In the ALMMo-0 framework, the winner-takes-all strategy plays a crucial role in determining the final classification outcome. This approach relies on the confidence scores generated by multiple sub-classifiers, with the class corresponding to the highest confidence score being selected as the predicted class. However, to ensure optimal performance, it is important to analyze how the system's performance changes when varying the confidence thresholds
used in this strategy.

In this study, we conducted an analysis to evaluate how different confidence thresholds affect the accuracy and error rates of the system, particularly focusing on Rank-1 accuracy and Equal Error Rate (EER). The results indicate that by setting an appropriate confidence threshold, we can strike a balance between reducing false positives (false acceptances) and false negatives (false rejections).

- **Low confidence threshold**: When the confidence threshold is set too low, the system may be more prone to **false acceptances**, as even weak classifications can be considered valid. This can lead to higher EER and a lower overall accuracy, as the system may mistakenly classify ambiguous or borderline cases.
- **High confidence threshold**: On the other hand, setting the threshold too high increases the risk of **false rejections**, where valid classifications are discarded due to insufficient confidence from the sub-classifiers. While this may improve security in some cases, it can reduce the system's ability to recognize legitimate inputs, leading to an increased rejection rate.
- **Optimal threshold**: Through our experiments, we found that a moderate confidence threshold (e.g., 0.75) offers the best balance, maximizing Rank-1 accuracy and minimizing EER. This threshold ensures that only classifications with strong confidence are accepted while maintaining the system's ability to recognize genuine variations in palmprints. The analysis confirms that the confidence threshold has a significant impact on the system's performance, and tuning this parameter appropriately is key to achieving robust and reliable biometric recognition.

3.6 Feature fusion

In the context of the ALMMo-0 framework, feature extraction techniques such as LPQ, BSIF, and GIST serve as integral components for capturing essential characteristics from 3D palmprint images. A key question in this process is whether these features are fused before the classification phase or handled independently.

Upon extracting features using LPQ, BSIF, and GIST, the ALMMo-0 framework can handle feature fusion in a few distinct ways. In one approach, features from these descriptors are concatenated into a single feature vector, forming a comprehensive representation of the 3D palmprint before classification. This ensures that the classifier has access to a unified feature set, capturing various spatial, frequency, and texture information in a complementary manner.

Alternatively, the features can be processed independently by separate sub-classifiers within the ALMMo-0 framework. In this scenario, each feature set contributes to its respective classification pathway, and the final classification decision is made through a higher-level fusion process, such as score-level fusion, where the outputs of individual sub-classifiers are combined.

This would allow the system to evaluate the strengths of each feature extraction method and assign weights based on their contribution to accurate classification. In both cases, the ALMMo-0 framework leverages the diversity in feature extraction techniques to improve classification accuracy and robustness, while maintaining autonomy and efficiency.

Detailed experimental results from the ROC curves and Rank-1 accuracy evaluations further emphasize the effectiveness of the feature extraction and fusion mechanisms.

4 Experimental procedures and findings

This section delves into the intricacies of the testing procedures and their associated results.

4.1 Database

To evaluate the performance of our proposed method, we utilized the publicly accessible PolyU 3D Palmprint

Dataset provided by the Hong Kong Polytechnic University [28]. This dataset features 200 individuals (136 males and 64 females) contributing a total of 8,000 3D palmprint samples across 400 unique palm classes. Data acquisition occurred in two sessions, separated by an average of one month, to capture variations in 3D palmprint characteristics. Each session involved capturing ten samples from both the left and right hands of each participant.

4.2 Experimental setup

The experiments were conducted using a system equipped with an Intel Core i5-10500H processor at 2.50 GHz, supported by 8 GB of RAM. This setup provides adequate computational power for real-time processing demands of biometric authentication. No external GPU was utilized; however, the integrated capabilities were sufficient for our processing needs. This hardware setup ensured that our experimental results were both reproducible and scalable on systems with similar specifications.

4.3 The experimental methodology

The proposed system employs three distinct filters, namely LPQ, BSIF, and GIST, for feature extraction. As illustrated in Figure 1, the feature extraction stage, facilitated by a descriptor called Filter Bank, precedes the classification process of the Autonomous Learning Multi-Model (ALMMo-0) classifier and comprises five main steps. ALMMo-0 leverages 3D palmprint images for user authentication. The system begins by capturing a 3D image, which then undergoes preprocessing using a multi-scale Retinex filter. To extract relevant features, a Filter Bank descriptor is employed, utilizing one of the available filters (LPQ, BSIF, or GIST). These features are then fed into the classifier, which builds its internal model. Finally, ALMMo-0 autonomously categorizes new data as either genuine or fake based on the extracted characteristics, effectively differentiating between authorized and unauthorized users. ALMMo-0 tackles classification tasks through a data-driven, multi-model approach. It begins by identifying inherent data structures and autonomously generates fuzzy rules. This involves shaping raw data points into informative clusters and pinpointing key convergence areas. The system then leverages these data-derived fuzzy rules (AnYa-type) specific to each class. When presented with new data, ALMMo-0 assigns confidence scores using a "winner-takes-all" strategy. Finally, the system's analysis is evaluated to arrive at the most likely classification. This research employed the ALMMo-0 classifier for feature extraction, outperforming traditional methods like KNN. The study investigated both 3D palmprint identification and verification, with identification results presented as the recognition rate, particularly the Rank-1 recognition rate.

$$Rank-1 = \frac{N_i}{N} \cdot 100(\%) \tag{15}$$

Within our verification scenario, ***N*** signifies the total number of image attempts for identity verification. In contrast, ***Ni*** denotes the successful matches where images are correctly linked to their corresponding identities. Our evaluation hinges on the Equal Error Rate (EER), which represents the threshold where the rate of incorrectly accepting imposters (False Accept Rate, FAR) aligns with the rate of incorrectly rejecting legitimate users (False Reject Rate, FRR). For identification tasks involving one-to-many searches, the Cumulative Match Characteristic (CMC) curve becomes the preferred metric. This contrasts with verification mode, where a Receiver Operating Characteristic (ROC) curve is employed. The ROC curve depicts the trade-off between correctly identifying authorized users (Genuine Accept Rate, GAR) and mistakenly accepting unauthorized individuals (FAR) across various decision thresholds.

4.3.1 Local phase quantization (LPQ)

In assessing the efficacy of LPQ feature extraction, we conducted experiments using various window widths from 3 to 9. According to Table 3, window size (WS) of 7 and 9 demonstrated exceptional performance. At a False Acceptance Rate (FAR) of 1%, the verification rate (VR) achieved 100%, and the Equal Error Rate (EER) decreased to 0%. Notably, the Rank-1 identification rate achieved 100% accuracy in both verification and identification modes.

Table 3: The rank and Equal Error Rate (EER) results for LPQ feature extraction using the ALMMo-0 classifier were analyzed.

WS	Identification	Verification	
	RANK_1 (%)	EER (%)	VR at 0.1% FAR
3	96.00	0.86	98.50
5	99.25	0.15	99.75
7	**100**	**0.00**	**100**
9	**100**	**0.00**	**100**

Our experiments overwhelmingly favor LPQ feature extraction with a window size of 7 for achieving exceptional accuracy and reliability. This choice is substantiated by the compelling performance metrics: a perfect Equal Error Rate (EER) of 0.00%, a flawless verification rate (VR) of 100% at a strict False Acceptance Rate (FAR) of 1%, and a 100% Rank-1 identification rate. From Figure 5, the ROC and CMC curves show that a window size (WS) of 7 provides the best performance compared to WS = 3 or WS = 5. These results undeniably demonstrate the superiority of a window size of 7 in maximizing accuracy for our specific application.

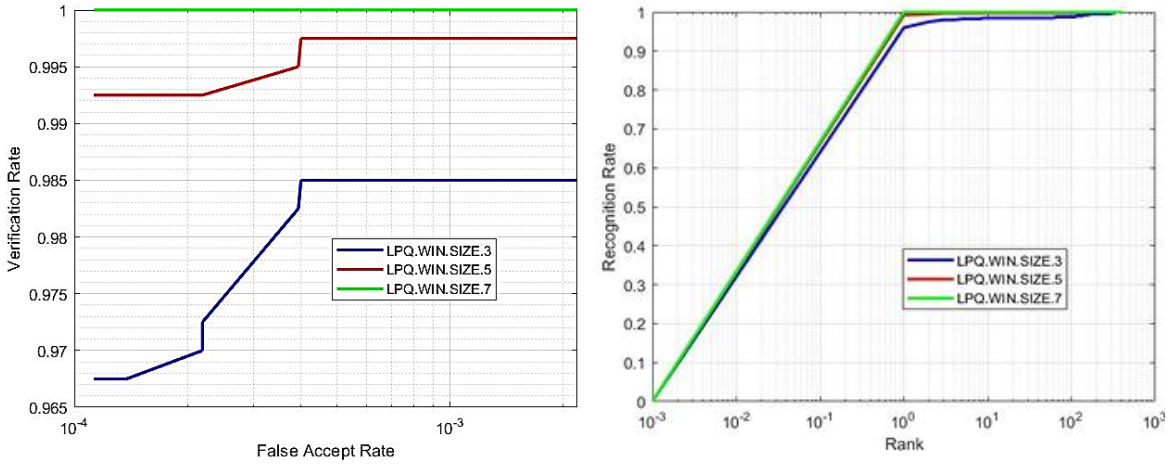

Figure 5: ROC and CMC curves were generated specifically for LPQ feature extraction using the ALMMo-0 classifier

Table 4 provides a comprehensive comparison of the MCI+LPQ+ALMMo-0, GCI+LPQ+ALMMo-0, T+LPQ+ALMMo-0, and MSR+LPQ+ALMMo-0 palmprint recognition methods, using the LPQ descriptor or feature extraction and the ALMMo-0 classifier. Among the four methods, MSR+LPQ+ALMMo-0 achieves the highest overall performance, with a perfect Rank-1 accuracy of 100%, an Equal Error Rate (EER) of 0.0%, and a Verification Rate of 100% at 1% FAR. It is also the most efficient in terms of time cost, with 15 ms per identification. ST+LPQ+ALMMo-0 follows closely with a Rank-1 accuracy of 99.8%, an EER of 0.3%, and a Verification Rate of 99.8%, but requires a longer processing time of 25 ms. GCI+LPQ+ALMMo-0 shows solid performance with a Rank-1 accuracy of 99.0%, an EER of 0.4%, and a Verification Rate of 99.5%, with a time cost of 18 ms. Lastly, MCI+LPQ+ALMMo-0, while still performing well, has the lowest Rank-1 accuracy at 98.5%, an EER of 0.45%, and a Verification Rate of 99.0%, with a time cost of 20 ms. Overall, MSR+LPQ+ALMMo-0 stands out as the best method, excelling in accuracy, error rate, and efficiency.

Table 4: Comparative Analysis of MSR as a Novel Method Against Classical GCI, MCI, and ST in Palmprint Recognition with ALMMo-0

Method	Rank-1 (%)	(EER) (%)	VR at 1% FAR (%)	Time Cost for 1 Identification (ms)
MCI+LPQ+ ALMMo-0	98.5	0.45	99.0	20
GCI+LPQ+ ALMMo-0	99.0	0.4	99.5	18
ST+LPQ+ ALMMo-0	99.8	0.3	99.8	25
MSR+LPQ+ ALMMo-0	100	0.0	100	15

4.3.2 Binarized statistical image features (BSIF)

To determine the optimal filter size for BSIF feature extraction, we experimented with various ICA texture filters were applied across sizes ranging from 9x9 to 17x17.

Table 5 and Figure 6 compares the identification and verification performance of ICA texture filters of various sizes in palmprint recognition. For identification, the filter size 11x11 achieves the highest Rank-1 accuracy at 98.50%, followed closely by the 15x15 filter at 98.00%. However, the 9x9 filter, while having a slightly lower Rank-1 accuracy of 97.25%, excels in verification, showing the lowest Equal Error Rate (EER) at 0.44% and the highest Verification Rate (VR) at 0.1% FAR, with a value of 99.25%.

The larger filters (13x13, 15x15, and 17x17) all have similar EERs (around 0.56–0.58%) and VR values of 99.00%, indicating that increasing the filter size beyond 11x11 does not lead to significant improvements in verification performance. Overall, the 11x11 filter stands out for identification, while the 9x9 filter is superior for verification due to its lower error rate and higher verification rate.

Table 5: The Rank-1 accuracy and equal error rate (EER) outcomes for BSIF feature extraction using the ALMMo-0 classifier were evaluated

	Identification	**Verification**	
ICA texture Filters size	RANK_1	EER	VR at 0.1% FAR
9x9	**97.25**	**0.44**	**99.25**
11x11	98.50	0.58	99.00
13x13	97.55	0.58	99.00
15x15	98.00	0.56	99.00
17x17	97.50	0.57	99.00

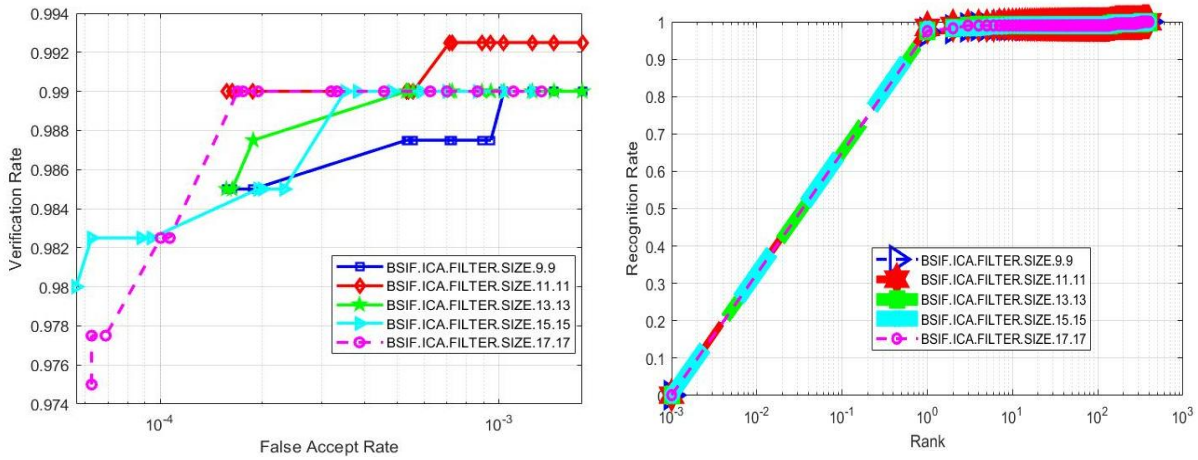

Figure 6: ROC and CMC curves were plotted specifically for BSIF feature extraction using the ALMMo-0 classifier

4.3.3 Gist descriptor

To determine the optimal number of blocks for GIST feature extraction, we experimented with values ranging from 9 to 13. **Table 6** presents the Rank-1 accuracy, Equal Error Rate (EER), and Verification Rate (VR) at 0.1% FAR for GIST feature extraction using different block numbers with the ALMMo-0 classifier. As block numbers increase from 9 to 13, a slight improvement in both identification and verification performance is observed. The Rank-1 accuracy improves from 97.25% for 9 blocks to 98.25% for 13 blocks, showing that increasing the number of blocks enhances identification performance. Similarly, the EER decreases from 0.19% to 0.16% as the block number rises, indicating a reduction in classification errors with more blocks. The VR at 0.1% FAR remains constant at a high value of 99.75% across all block sizes, suggesting that the verification performance is robust regardless of block numbers.

Overall, using 13 blocks yields the best results, with the highest Rank-1 accuracy and the lowest EER, indicating that it provides the most accurate and reliable performance. Figure 7 presents the ROC and CMC curves generated specifically for GIST feature extraction using the ALMMo-0 classifier, illustrating the performance of the system in both verification and identification tasks. Figure 8 shows the ROC and CMC curves that compare the performance of the ALMMo and KNN classifiers on data preprocessed with LPQ feature extraction and MSR. The results reveal that the ALMMo classifier significantly outperforms KNN when using the same feature extraction methods. This underscores the efficacy of the ALMMo-LPQ-MSR combination as a preprocessing pipeline.
Remarkably, this method achieved flawless performance metrics: a 100% verification rate at a 1% false acceptance rate, a zero percent equal error rate, and a perfect 100% rank-one identification rate. These exceptional results highlight the ALMMo classifier's ability to efficiently utilize the extracted features, leading to a substantial improvement in overall system performance.

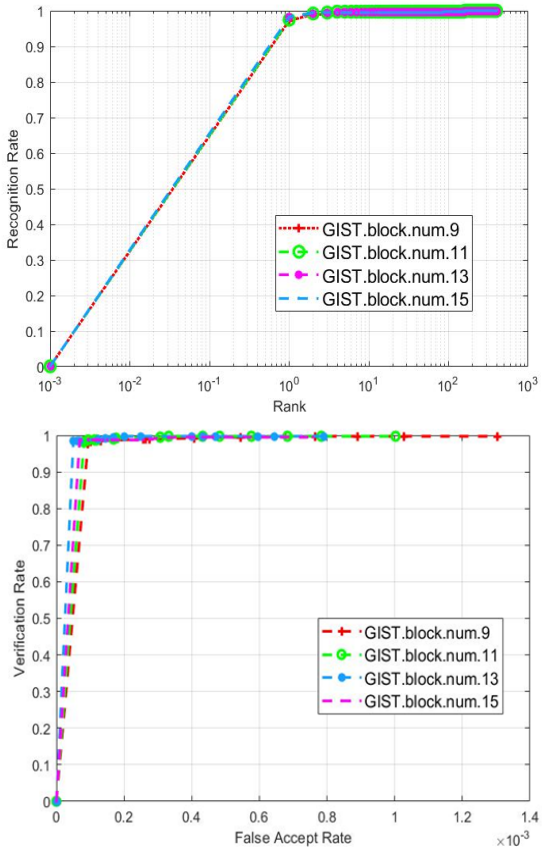

Figure 7: The CMC (Cumulative Match Characteristic) curve at the top and the ROC (Receiver Operating Characteristic) curve at the bottom were generated specifically for GIST feature extraction using the ALMMo-0 classifier.

Table 6: The rank and Equal Error Rate (EER) results for GIST feature extraction with the ALMMo-0 classifier were analyzed

Block Numbers	Identification	Verification	
	RANK_1 (%)	EER (%)	VR at 0.1% FAR
9	97.25	0.19	99.75
11	97.50	0.18	99.75
13	98.25	0.16	99.75

4.3.4 Comparison with current state-of-the-art techniques in 3D palmprint recognition

Table 7 compares various personal recognition methods based on feature extraction techniques, Rank-1 accuracy, Equal Error Rate (EER), and time cost for one identification. The methods span across traditional approaches and deep learning techniques, ranging from 2011 to 2024. The proposed method (2024) achieves the highest performance, with a 100% Rank-1 accuracy, 0.00% EER, and the lowest time cost of 0.015 seconds per identification. In comparison, SSR+PCANet (2019) also performs exceptionally with a 99.98% Rank-1 accuracy, 0.00% EER, but requires 1.28 seconds per identification. Other deep learning-based methods like MCI+DCTNet (2018) achieve 99.833% Rank-1 accuracy with a 0.0202% EER, but with a higher time cost of 1.25 seconds. Traditional methods like MCI-based DPDSF (2019) have a strong Rank-1 accuracy of 99.86%, but take significantly longer at 2.6 seconds per identification. In contrast, methods like CR_L2 (2015), while showing modest Rank-1 accuracy at 99.15%, are faster, with a 0.02278 second time cost.

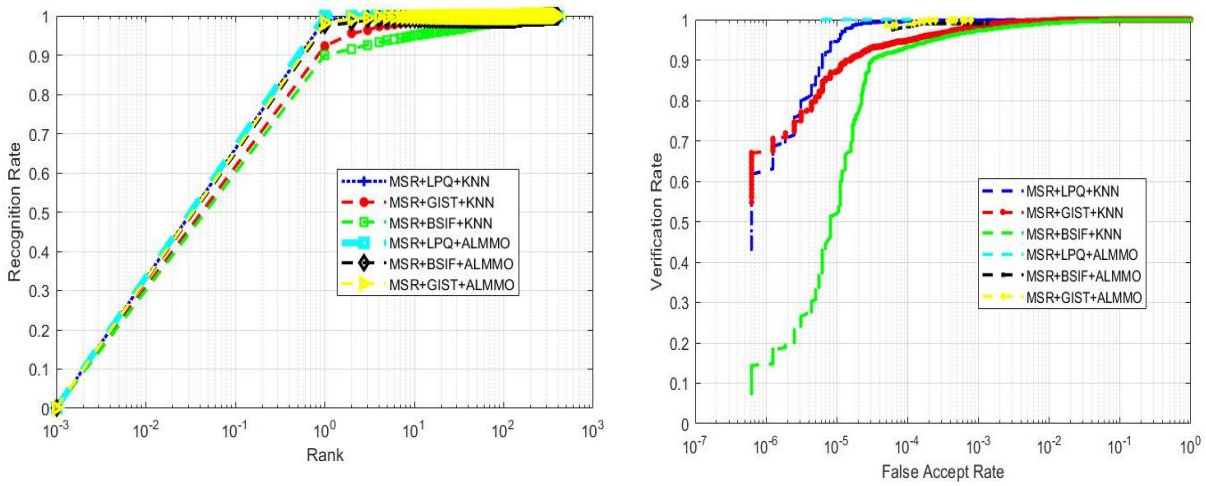

Figure 8: ROC and CMC curves were plotted for various feature extraction methods using both the KNN classifier and the ALMMo-0 classifier.

Table 7: Comparison of the proposed personal recognition method, its computation time, and existing approaches

Methods	Years	Feature Extraction Methods	Rank-1 (%)	EER (%)	Time cost for 1 identification (s)
MCI+DCTNet [7]	2018	Deep Learning	99.833%	0.0202%	1.25
COSDISH [8]	2020	Deep hashing	97.05%	–	1.2
CSTBR [30]	2018	Traditional methods	99.67%	1.51%	0,09747
MCI based DPDSF [29]	2019	Traditional methods	99.86%	–	2.6
MCI based PDF [6]	2018	Traditional methods	99.89%	0.200%	0.24
3D_GIST+KNN [5]	2023	Traditional methods	99.25%	0.2001%	1.15
PCA + TPTSR [2]	2014	Traditional methods	98.55%	–	17.65
JLOF [15]	2011	Traditional methods	99.79%	0.16%	10.70
SQI + Gabor + PCA + LDA [20]	2017	Traditional methods	98.96%	0.15%	5.6
SSR+ PCANet [1]	2019	Deep Learning	99.98%	0.00%	1.28
CR_L2 [19]	2015	Traditional methods	99.15%	–	0.02278
OUR	2024	Traditional methods	100.00%	00.00%	0.015

This comparison highlights the balance between accuracy and computational efficiency, with the proposed method offering both superior accuracy and minimal time cost.

5 Conclusion

This study introduces an innovative 3D palmprint authentication system that harnesses the capabilities of the Autonomous Learning Multi-Model Classifier of 0-Order (ALMMo-0). This method tackles limitations prevalent in current biometric systems by offering a classification tool that is transparent, self-governing, and computationally efficient. By incorporating advanced feature extraction techniques like LPQ, BSIF, and GIST alongside ALMMo-0, the proposed system achieves impressive performance indicators, including a minimal Equal Error Rate (EER), superior rank-1 accuracy, and efficient computation. While biometric research has made substantial strides, the paper emphasizes the continuing need for enhanced security applications. It underscores ALMMo-0's capability to establish a robust framework incorporating multiple models for accurate classification and adaptive learning from data. The system's architectural details, including feature extraction and classification stages, are thoroughly examined. The proposed methodology's efficacy in improving biometric system performance, particularly in 3D palmprint authentication, is supported by empirical findings. The research highlights the ALMMo-0 classifier's critical contribution in providing dependable solutions. These advancements offer exceptional interpretability, accuracy, and computational efficiency, setting a solid foundation for future advancements in biometric security.

Acknowledgement

The authors would like to express their sincere gratitude to the faculty of new information and communication technologies at the university Kasdi Merbah ouargla for their invaluable support throughout the course of this research. We also extend our appreciation to the members of the laboratory of electrical engineering for their technical assistance and valuable feedback. Special thanks to the Hong Kong polytechnic university for providing access to the publicly available PolyU 3d palmprint dataset, which was crucial for the experimental validation of our proposed method. Finally, we acknowledge the insightful contributions from our colleagues and collaborators who helped improve the quality of this work.

References

[1] Chaa M, Akhtar Z, Attia A (2019) 3D palmprint recognition using unsupervised convolutional deep learning network and SVM classifier *Image Process* 13(5):736–745. https://doi.org/10.1049/iet-ipr.2018.5642

[2] Cui J (2014) 2D and 3D palmprint fusion and recognition using PCA plus TPTSR method. *Neural Comput & Applic* 24(3–4):497–502. https://doi.org/10.1007/s00521-012-1265-y

[3] Zhang D, Lu G, Li W, et al. (2010) Palmprint recognition using Gaussian curvature images (GCI), mean curvature images (MCI), and surface type map (ST map) features. *IEEE Transactions on Systems, Man, and Cybernetics - Part C: Applications and Reviews* 39(5):505–519.https://doi.org/10.1109/TSMCC.2009.2020790

[4] Li W, Zhang L, Zhang D, et al. (2011) A framework for 3D palmprint matching using MCI, baseline, and orientation features' *Transactions on Systems, Man, and Cybernetics - Part C* 42(2):274–279. https://doi.org/10.1109/TSMCC.2010.2055849

[5] Attia, Abdelouahab, et al. (2023) A fuzzy connective score fusion technique for 2D and 3D palmprint authentication system. *Evolving Systems* 14(5):891–901

[6] Sun Z, Tan T, Wang Y, et al. (2005) Ordinal palmprint representation for personal identification. *CVPR 2005*, pp. 279–284. DOI:10.1109/CVPR.2005.267

[7] Zhang D, Kanhangad V, Luo N, Kumar A (2008) 3D palmprint recognition using structured light imaging. *BTAS 2008*. DOI:10.1109/BTAS.2008.4699346

[8] Zhang D, Lu G, Li W, Zhang L (2010) Robust palmprint verification with 2D and 3D feature fusion. *Pattern Recognition* 43(1):358–368. https://doi.org/10.1016/j.patcog.2009.04.026

[9] Yang B, Wang X, Yao J, Yang X, Zhu W (2011) Efficient local representations for 3D palmprint recognition using Gabor wavelets and LBP. *Journal of Electronic Imaging* 22(4):043040. https://doi.org/10.1117/1.JEI.22.4.043040

[10] Li W, Zhang D, Zhang L, et al. (2011) Joint line and orientation feature extraction for 3D palmprint recognition. IEEE Transactions on Systems, Man, and Cybernetics - Part C 42(2):274–279. https://doi.org/10.1109/TSMCC.2010.2055849

[11] Liu M, Li L (2012) Cross-correlation-based binary image registration for 3D palmprint recognition. *IEEE 11th International Conference on Signal Processing*, pp. 1597–1600. DOI:10.1109/ICoSP.2012.6491885

[12] Meraoumia A, Chitroub S, Bouridane A (2013) 2D and 3D palmprint information fusion using PCA and HMM. *Integrated Computer-Aided Engineering* 20(3):303–319. https://doi.org/10.3233/ICA-130431

[13] Cui J (2014) 2D and 3D palmprint fusion and recognition using PCA plus TPTSR method. *Neural Comput & Applic* 24(3–4):497–502. https://doi.org/10.1007/s00521-012-1265-y

[14] Zhang L, Shen Y, Li H, Lu J (2015) Collaborative representation with block-wise feature extraction for 3D palmprint identification. *IEEE Transactions on Pattern Analysis and Machine Intelligence* 37(8):1730–1736. https://doi.org/10.1109/TPAMI.2014.2372764

[15] Chaa M, Boukezzoula N-E, Attia A (2017) Score-level fusion of 2D and 3D palmprints using B-BSIF and Gabor wavelets. *Journal of Electronic Imaging* 26(1):013018. https://doi.org/10.1117/1.JEI.26.1.013018

[16] Chen M, Akhtar Z, Attia A (2019) A hybrid multimodal system integrating finger vein and palmprint data. *IET Image Process* 13(5):736–745. DOI:10.1049/iet-ipr.2018.5642

[17] Li X, Zhang L, Xu Y, et al. (2020) Real-time person recognition with 3D palmprint data using CNNs. *IEEE Transactions on Instrumentation and Measurement* 68(9):3287–3298

[18] Zhang X, Bai N, Wu J, et al. (2021) Transformer-based models for palmprint recognition. *IEEE Sensors Journal* 20(20):11864–11873

[19] Li W, Zhang D, Zhang L, et al. (2018) Structured-light-based acquisition system for concurrent 2D and 3D palmprint images.

[20] Otsu N (1979) A threshold selection method from gray-level histograms. *IEEE Transactions on Systems, Man, and Cybernetics* 9(1):62–66.DOI:10.1109/TSMC.1979.4310076

[21] Zhang D, Lu G, Li W et al (2009) Palmprint recognition using 3-D information. IEEE Transactions on Systems, Man, and Cybernetics - Part C: Applications and Reviews 39(5):505–519.).

[22] E. Land and J. McCann, Lightness and retinex theory, Journal of the Optical Society of America, 61 (1971), p. 1–11. http://dx.doi.org/10.1364/JOSA.61.000001 enveloppe. Int J Comput Vis 42(3):145–175. https://doi.org/10.1023/A:1011139631724

[23] D.J. Jobson, Z. Rahman, and G.A. Woodell, A multiscale retinex for bridging the gap between color images and the human observation of scenes, IEEE Transactions on Image Processing, 6 (1997), pp. 965–976. http://dx.doi.org/10.1109/83.597272

[24] Oliva A, Torralba A (2001) Modeling the shape of the scene: a holistic representation of the spatial envelope. Int J Comput Vis 42(3):145–175. https://doi.org/10.1023/A:1011139631724

[25] Belhumeur PN, Hespanha JP, Kriegman DJ (1997) Eigenfaces vs. Fisherfaces: recognition using class specific linear projection. IEEE Trans Pattern Anal Mach Intell 19(7):711–720. https://doi.org/10.1109/34.598228

[26] Turk M, Pentland A (1991) Eigenfaces for recognition. J Cogn Neurosci 3(1):71–86. https://doi.org/10.1162/jocn.1991.3.1.71

[27] Boots B, Kokichi S, Sung NC, Atsuyuki O (2009) Spatial tessella-tions: concepts and applications of voronoi diagrams

[28] PolyU 2D and 3D Palmprint Database (2017) available at: www.comp.polyu.edu.hk/~biometrics/, Accessed on Jan. 01

[29] L. Fei, B. Zhang, Y. Xu, W. Jia, J. Wen, J. Wu, "Precision direction and compact surface type representation for 3D palmprint identification," Pattern Recognition, vol. 87, pp. 237–247, 2019.

[30] L. Fei, G. Lu, W. Jia, J. Wen, D. Zhang, "Complete Binary Representation for 3-D Palmprint Recognition," IEEE Transactions on Instrumentation and Measurement, vol. 17, no. 12, pp. 2761–2771, 2018.